Available online at www.sciencedirect.com
ScienceDirect
Ceramics International 37 (2011) 49–53
CERAMICS INTERNATIONAL
www.elsevier.com/locate/ceramint

Structure, thermal stability and electrical conductivity of $CaMoO_{4+\delta}$

H.-N. Im, M.-B. Choi, S.-Y. Jeon, S.-J. Song *

Department of Materials Science and Engineering, Chonnam National University, 300 Yongbong-dong, Buk-gu, Gwangju 500-757, South Korea

Received 28 May 2010; received in revised form 14 June 2010; accepted 13 July 2010
Available online 7 August 2010

Abstract

Single-phase tetragonal scheelite $CaMoO_4$ (space group, *Pmmm*) was prepared via the conventional solid state reaction method. The oxidation state of the transition metal species for the as-sintered $CaMoO_4$ was analyzed by X-ray photoelectron spectroscopy (XPS). The average thermal expansion coefficient was measured as about $11 \times 10^{-6}\ K^{-1}$ over the temperature range of 303–1373 K. From the thermodynamic point of view, the phase diagram for $CaMoO_4$ was constructed by computing the equilibrium phase boundaries. Finally, the electrical conductivity of $CaMoO_4$ was also investigated by an AC impedance analyzer. The activation energy of bulk conductivity for $CaMoO_4$ was 2.1 eV.

Keywords: C. Thermal expansion; Scheelite; Chemical stability

1. Introduction

In the scheelite structure, the Ca^{2+} exists as a bisdisphenoid polyhedron with eight oxygen atoms forming a CaO_8 polyhedron, whereas the molybdenum (Mo) ions are surrounded by four oxygen atoms forming a tetrahedral unit. The CaO_8 polyhedron shares four of its edges with four other CaO_8 polyhedra extending in the *c*-directions. Each oxygen atom of the CaO_8 polyhedron is connected to one Mo atoms [1–4]. Especially, Mo containing scheelite type ABO_4 compounds has been of interest for decades, not only because of its excellent optical properties suitable for phosphors, lasers, optical fibers, and electrochromic materials, but also due to its mixed conducting properties for negative electrode materials in Li-ion batteries [5–8]. Recently, the reduced structure of perovskite, $CaMo_{0.5}V_{0.5}O_3$, has become recognized as a promising anode material for replacing Ni-YSZ cermet anode in solid oxide fuel cells (SOFC) because of its good mixed conduction, comparable thermal expansion with Ni-YSZ, and oxygen exchange catalytic properties [9–11]. Even though the point-defect related conductivity itself is an important parameter for understanding the defect chemistry and optimizing the electrochemical device operation, very few reports [12] have attempted such optimization. Due to the difficulty in preparing single-phase $CaMoO_3$ perovskite, the $CaMoO_4$ reduction to $CaMoO_3$ has been generally accepted as a cost-effective, efficient processing route. However, the basic material properties of $CaMoO_4$, including phase stability and electrical properties, have not been thoroughly investigated.

This study aimed to determine the conductivity behavior of $CaMoO_4$ in a N_2–O_2 atmosphere at various temperatures. The thermal expansion coefficient was measured to confirm the loss of lattice oxygen from thermal gravimetric and differential thermal analysis (TG/DTA) measurements as a function of temperature and the scheelite phase stable regime was calculated.

2. Experimental

Scheelite $CaMoO_4$ powders were prepared by the citric acid method. $CaCO_3$ (Aldrich, 99.99%), and $(NH_4)_6Mo_7O_{24.4}H_2$ (Aldrich, 99.99%) were dissolved in 10% citric acid. The mixed solution was dried at 393 K for 12 h for dehydration and then heated at 873 K for 8 h and reheated at 1073 K for 2 h in air. The calcined oxide powders were then crushed, sieved to <45 μm, pressed into pellets, cold-isostatic-pressed, and sintered at 1273 K for 10 h in air for conductivity measurements. The obtained powders were characterized by X-ray diffraction (XRD;

* Corresponding author. Tel.: +82 62 530 1706; fax: +82 62 530 1699.
E-mail address: song@chonnam.ac.kr (S.J. Song).

0272-8842/$36.00
doi:10.1016/j.ceramint.2010.08.004

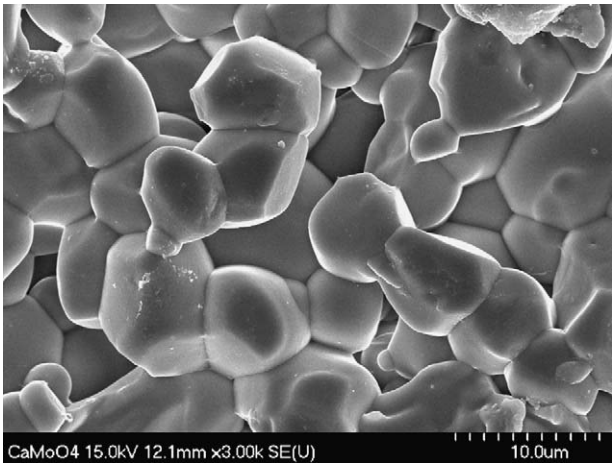

Fig. 1. Scanning electron micrograph (SEM) of polished fracture surface of $CaMoO_4$ sintered at 1273 K in air.

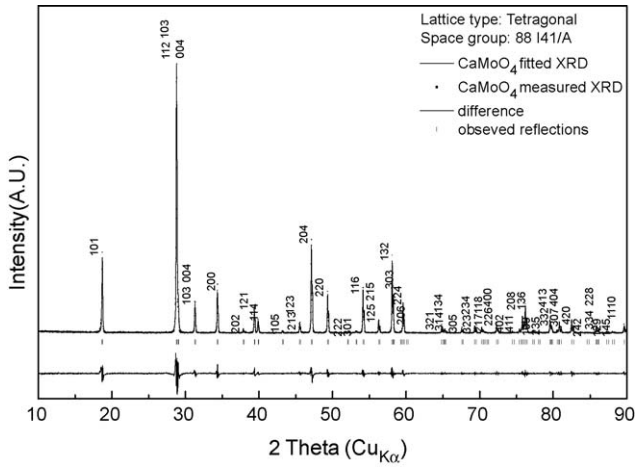

Fig. 2. Room temperature X-ray diffraction (XRD) patterns of $CaMoO_4$ sintered at 1273 K in air.

D/MAX Ultima III, Rigaku, Japan) equipped with a Cu target X-ray tube at a scan rate of 1°/min between scanning angles of (2θ) 10° and 90°. The obtained XRD pattern was refined using the Full-Prof program according to the Rietveld method [13]. The scanning electron micrograph (SEM; Shimadzu, SS-550) image of the as-sintered fracture surface, in Fig. 1, shows well developed grains and low porosity.

TG/DTA was performed with SDT Q600 V8.0 Build 95 thermal analyzer at a heating rate of 10 K/min from room temperature to 1273 K in air with 100 cc/min flow rate. The oxygen partial pressure (pO_2) was monitored before and after the thermal analysis with a zirconia oxygen sensor. X-ray photoelectron spectroscopy (XPS) analysis was performed using a VG Multilab 2000 spectrometer (Thermo VG Scientific) in an ultra high vacuum. This system uses an unmonochromatized Mg K_α (1253.6 eV) source and a spherical section analyzer. Survey scan data and core peak data were collected using pass energies of 50 and 20 eV, respectively. No charge neutralization was used. The binding energy scale was calibrated from the hydrocarbon contamination using the C 1s peak at 284.5 eV. All binding energies obtained in this study were precise to within ±0.2 eV.

For AC electrical measurements, pellets were coated with Pt-paste (Engelhard 6926) and heated to 1173 K for 1 h. Conductivity measurements were performed with a Solartron 1260 Impedance Analyser in the frequency range of 0.1 Hz to 1 MHz at an amplitude of 100 mV in a temperature range of 773–1173 K. Various pO_2 values, obtained by mixing O_2 and N_2, were measured by a zirconia oxygen sensor [14]. Thermal expansion was measured using a Netzch L75 PT1600 dilatometer from room temperature to 1273 K at 2 °C/min with an air purge at a flow rate of 50 cc/min of air, N_2, and 5% H_2 balance by N_2 conditions.

3. Results and discussion

As shown in Fig. 2, XRD spectra confirmed the attainment of single-phase tetragonal scheelite $CaMoO_4$ (space group, *Pmmm*). No peaks of any other planes were detected, indicating the high purity of the product. The refined XRD pattern is also depicted in Fig. 2. However, the results of line profiling analysis may not be completely reliable because of the relatively fast scan rate (1 K/min). The refined unit cell parameters for $CaMoO_4$ at ambient temperature are: $a = 5.222$ Å, $b = 5.222$ Å, and $c = 11.425$ Å ($V = 311.55$ Å^3), which is in agreement with previous reports [1,3].

To elucidate the oxidation state of the transition metal species in the prepared samples, XPS analysis was carried out and the result is shown in Fig. 3. A non-linear, least-squares fitting algorithm was used to deconvolute the peaks. The spectrum for the as-sintered $CaMoO_4$ in the Mo 3d region showed the presence of two well resolved spectral lines at 232.6 and 235.8 eV, which were assigned to the binding energies of an electron in Mo $3d_{5/2}$ and Mo $3d_{3/2}$, spin–orbit components, respectively (see Fig. 3a). The observed values suggest that the valence state of Mo in the sample is mainly +6, which is consistent with the previous XPS results [15–17]. Even though the assignment of the oxygen species is not yet well established, literature reports indicate that the peaks at ∼ 530 eV (O 1s-*a* = 530.5 eV, and O 1s-*b*+ 529.24 eV) are due to oxides, as shown in Fig. 3b.

Fig. 4a shows the thermal expansion curves and pO_2 values of the down-stream gas of $CaMoO_4$ at various pO_2 levels (air, N_2, 5% H_2 balance by N_2). The plot exhibits a linear expansion with temperature over the temperature range of 303–1373 K. The average thermal expansion coefficient is about 11×10^{-6} K^{-1} between 323 and 1073 K for all three atmospheres. Due to the nature of the tetragonal structure, Achary et al. reported that the variation of the CaO_8 polyhedra and the volume of the rigid immobile MoO_4 tetrahedra indicated that the *c*-axis should have a higher expansion as the CaO_8 polyhedra are closely connected along the *c*-axis. No inflexions were noticed but the deviation from linearity was revealed above 1073 K in 5%H_2 balance N_2 conditions. The thermal expansion trends agreed well with the TG/DTA results of the $CaMoO_4$ powders, as shown in Fig. 4b. The significant weight loss above 1073 K was measured without any specific peak of reaction. The

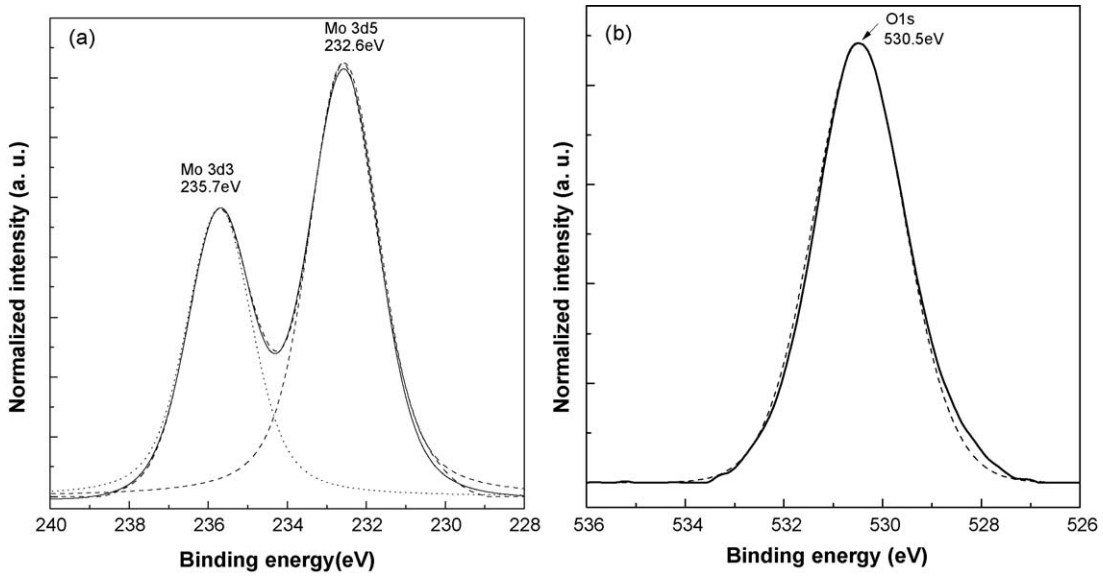

Fig. 3. X-ray photoelectron spectroscopy (XPS) spectra of (a) the Mo 3d doublet, and (b) oxygen in $CaMoO_4$ sintered at 1273 K in air.

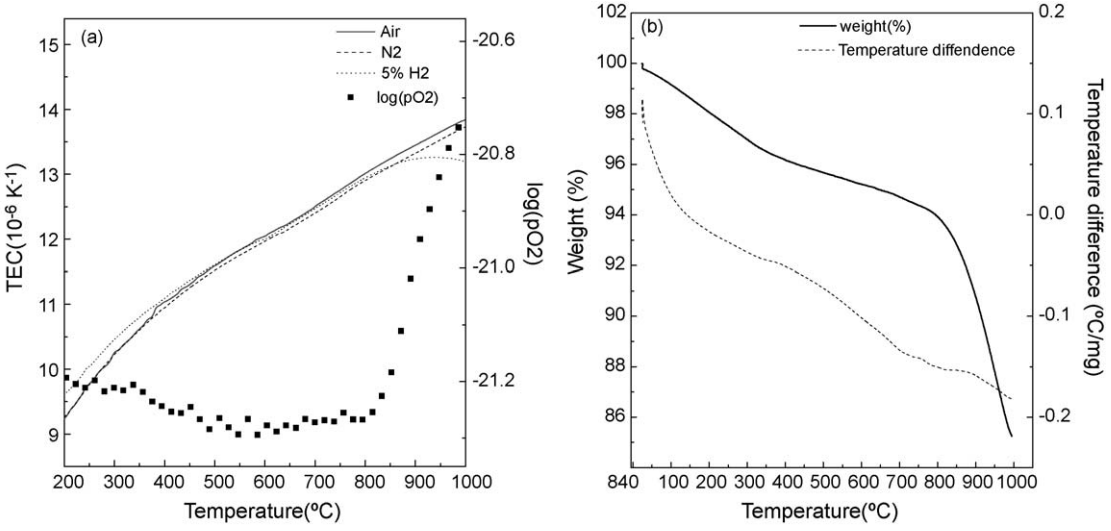

Fig. 4. (a) Oxygen partial pressure (pO_2) and thermal expansion curve for $CaMoO_4$ in the temperature range of 303–1273 K, and (b) TG/DTA curve for $CaMoO_4$.

deviation may be interpreted as the thermally induced loss of lattice oxygen, leading to the formation of oxygen vacancies due to Mo cation reduction for charge neutrality. This explanation was confirmed by the ex situ pO_2 measurement, as shown in Fig. 3(a). In the 5% H_2 balance N_2 condition, the down-stream pO_2 was around −21.2 in logarithm scale, but then increased to −20.8 above 1073 K, suggesting the emission of the lattice oxygen. The XRD spectra, as shown in Fig. 5, also confirmed the formation of second-phase perovskite $CaMoO_3$ due to the chemical reduction after the heat treatment in the 5% H_2 balance N_2 condition. From the thermodynamic point of view, with consideration for the reaction with the atmosphere, the predominance diagram for $CaMoO_4$ was constructed by computing the equilibrium phase boundaries, as shown in Fig. 6. This figure shows that $CaMoO_4$ may be reduced to $CaMoO_3$ at pO_2 below 10^{-17} atm at 1173 K.

Fig. 7(a) shows the AC impedance results, along with the equivalent circuit used in fitting. The impedance response of the $CaMoO_4$ samples according to measured temperature typically showed a single overlapped arc in the Nyquist plot, related to the electrode response [18]. Due to the similar capacitance of the bulk/grain boundary over the studied temperature range, the high frequencies intercept at the overlapped arc could not be further analyzed. The Arrhenius plot of the electrical conductivity is shown in Fig. 7(b). The total conductivity was in good agreement with the literature values over the measured temperature range for $CaMoO_4$. The calculated activation energy, consisting of the formation and migration energy for mobile defect species, was 2.1 eV.

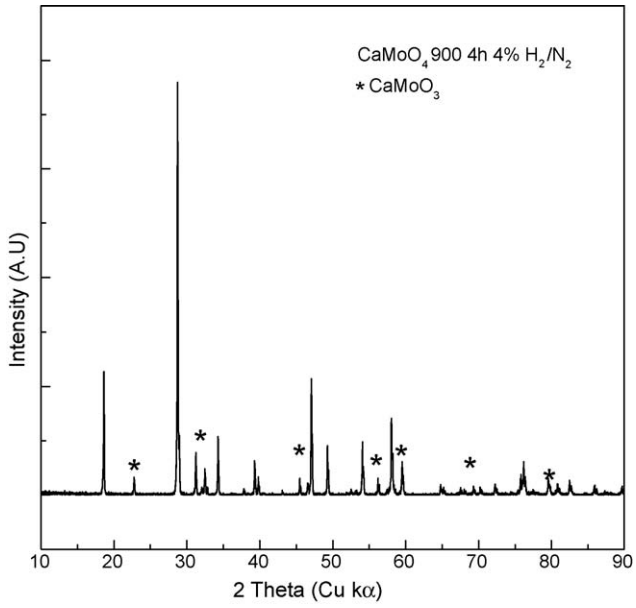

Fig. 5. Room temperature X-ray diffraction (XRD) patterns of $CaMoO_4$ after heat treatment at 1173 K in 5% H_2 balance by N_2 condition.

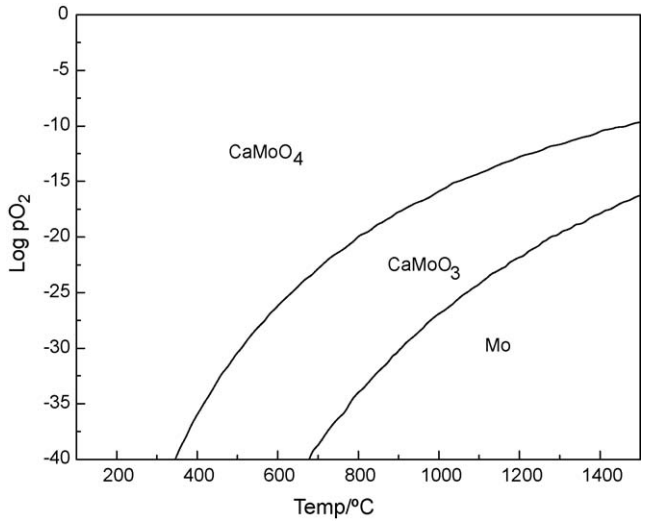

Fig. 6. Predominance phase diagram of $CaMoO_4$.

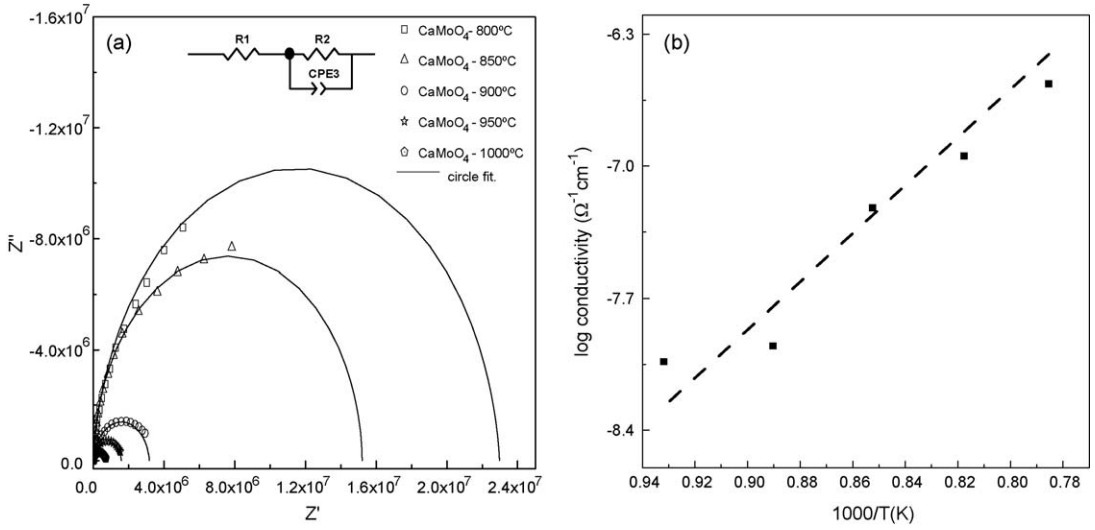

Fig. 7. (a) Typical AC impedance profiles of $CaMoO_4$ at various temperatures, and (b) logarithm of the electrical conductivity of $CaMoO_4$ as a function of temperature.

4. Conclusions

Single-phase tetragonal scheelite $CaMoO_4$ (space group, *Pmmm*) was prepared via conventional solid state reaction method. The refined unit cell parameters for $CaMoO_4$ at ambient temperature were: $a = 5.222$ Å, $b = 5.222$ Å, and $c = 11.425$ Å ($V = 311.55$ Å^3). The oxidation state of the transition metal species for the as-sintered $CaMoO_4$ was analyzed by XPS. The two well resolved spectral lines at 232.6 and 235.8 eV were assigned to the binding energies of an electron in Mo $3d_{5/2}$ and Mo $3d_{3/2}$, spin–orbit components, respectively. The average thermal expansion coefficient was about 11×10^{-6} K^{-1} over the temperature range 303–1273 K. From the thermodynamic point of view, the predominance diagram for $CaMoO_4$ was constructed by computing the equilibrium phase boundaries, suggesting that $CaMoO_4$ may be reduced to $CaMoO_3$ at pO_2 below 10^{-17} atm at 1173 K. The electrical conducting properties of $CaMoO_4$ were also investigated by an AC impedance analyzer. The activation energy of bulk conductivity for $CaMoO_4$ was 2.1 eV.

Acknowledgement

This work was supported by Solid Oxide Fuel Cell of Mew & Renewable Energy R&D Program (20093021030010) under the Korea Ministry of Knowledge Economy (MIKE).

References

[1] S.N. Achary, S.J. Patwe, M.D. Mathews, A.K. Tyagi, J. Phys. Chem. Sol. 67 (2006) 774–781.
[2] A. Senyshyn, H. Kraus, V.B. Mikhailik, L. Vasylechko, M. Knapp, Phys. Rev. B 73 (2006) 0141041–0141049.
[3] W.A. Crichton, A. Grzechnik, Z. Kristallogr. NCS 219 (2004) 337–338.
[4] G. Wandahl, A.N. Christensen, Acta Chem. Scand. A41 (1987) 358–360.
[5] G.K. Choi, S.-Y. Cho, J.-S. An, K.-S. Hong, J. Eur. Ceram. Soc. 26 (2006) 2011–2015.
[6] N. Sharma, K.M. Shaju, G.V. Subba Rao, B.V.R. Chowdari, Z.L. Dong, T.J. White, Chem. Mater. 16 (2004) 504–512.
[7] L.F. Johnson, G.D. Boyd, K. Nassau, R.R. Soden, Phys. Rev. 126 (4) (1962) 1406–1409.
[8] S.-S. Kim, S. Ogura, H. Ikuta, Y. Uchimoto, M. Wakihara, Solid State Ionics 146 (2002) 249–256.
[9] A. Aguadero, C.D. Calle, J.A. Alonso, D. Perez-Coll, M.J. Escudero, L. Daza, J. Power Sources 192 (2009) 78–83.
[10] K. Kamata, T. Nakamura, T. Sata, Chem. Lett. (1975) 81–86.
[11] C.D. Calle, J.A. Alonso, M. Garcia-Hernandez, V. Pomjakushin, J. Solid State Chem. 179 (2006) 1636–1641.
[12] A. Petrov, P. Kofstad, J. Solid State Chem. 30 (1979) 83–88.
[13] M.B. Choi, S.-Y. Jeon, H.-J. Hwang, S.-J. Song, J. Power Sources 195 (2010) 1059–1064.
[14] C.-J. Park, H.-R. Ryu, J.-H. Moon, S.-J. Song, Ceram. Int. 35 (2009) 1769–1773.
[15] J.-G. Choi, L.T. Thompson, Appl. Surf. Sci. 93 (1996) 143–1498.
[16] G.-T. Kim, T.-K. Park, H. Chung, Y.-T. Kim, M.-H. Kwon, J.-G. Choi, Appl. Surf. Sci. 152 (1999) 35–43.
[17] Z.B. Zhaobin Wei, P. Grange, B. Delmon, Appl. Surf. Sci. 135 (1998) 107–114.
[18] S.-J. Song, J.-H. Moon, T.-H. Lee, S.E. Dorris, U. Balachandran, J. Ceram. Process. Res. 9 (4) (2008) 376–380.